ACS OMEGA

Open Access

http://pubs.acs.org/journal/acsodf

Article

Bifunctional Copper Chelators Capable of Reducing Aβ Aggregation and Aβ-Induced Oxidative Stress

Olga Krasnovskaya,* Daniil Abramchuk, Alexander Vaneev, Petr Gorelkin, Maxim Abakumov, Roman Timoshenko, Ilia Kuzmichev, Nelly Chmelyuk, Veronika Vadehina, Regina Kuanaeva, Evgeniy Dubrovin, Vasilii Kolmogorov, Elena Beloglazkina, Olga Kechko, Vladimir Mitkevich, Kseniya Varshavskaya, Sergey Salikhov, and Alexander Erofeev*

Cite This: *ACS Omega* 2024, 9, 43376−43384

Read Online

ACCESS | Metrics & More | Article Recommendations | Supporting Information

ABSTRACT: Five bifunctional copper chelating agents, **Alz-(1−5)**, designed to prevent beta-amyloid (Aβ) aggregation, were synthesized, and the leader compound (**Alz-5**) was chosen. **Alz-5** acts as a bifunctional chelator that can interact with various Aβ aggregates and reduce their neurotoxicity. Reactive oxygen species measurements provided by the Pt-nanoelectrode technique in single $A\beta_{42}$-affected human neuroblastoma SH-SY5Y cells revealed significant antioxidant activity of **Alz-5**. AFM data obtained on $A\beta_{42}$ fibrils clearly indicate the antiaggregating property of **Alz-5**. To gain insights into the changes in the physiomechanical properties of $A\beta_{42}$-affected cells, as well as in order to evaluate the antiaggregating ability of **Alz-5**, Young's modulus mapping on living SH-SY5Y cells affected consequently by $A\beta_{42}$ and **Alz-5** was conducted, and the ability of **Alz-5** to decrease cell rigidity induced by $A\beta_{42}$ was indisputably proven. Low cell toxicity and antioxidating properties, in conjunction with AFM and SICM-based biophysical provided on $A\beta_{42}$-affected SH-SY5Y cells, support **Alz-5** as a potential inhibitor of Aβ aggregation.

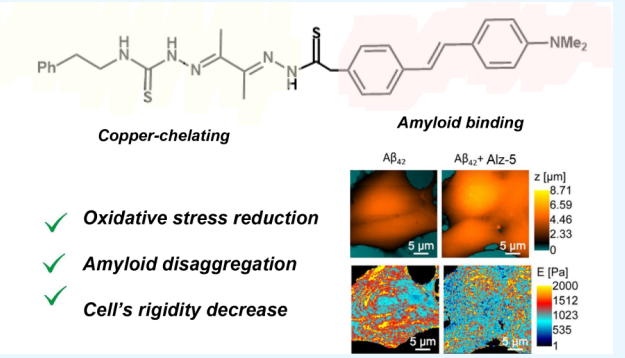

INTRODUCTION

Alzheimer's disease (AD) is the most common neurodegenerative disorder, which is characterized by intracerebral β-amyloid (Aβ) aggregation, τ-hyperphosphorylation, and loss of cholinergic neurons.[1] The other important hallmarks of AD are oxidative stress, metal dyshomeostasis, and inflammation.[2,3]

A breakdown in metal homeostasis is an important therapeutic target used in the development of anti-AD drugs.[4] AD-affected brains are associated with high concentrations of copper, iron, and zinc in Aβ structures.[5,6] Metal ions are key players modulating Aβ self-assembly and associated toxicity; redox-active copper cations promote reactive oxygen species (ROS) formation.[7−11] The involvement of Cu^{2+} in AD pathogenesis is supported by the fact that Cu^{2+} ions form a high-affinity complex with Aβ via binding with D1, H6, and H13 or H14 residues in amyloid fibrils and promote its aggregation.[12−14]

The use of metal chelation agents is a promising AD treatment strategy.[15] Metal chelators can reduce Aβ aggregation, ROS formation, and neurotoxicity in vitro.[16] Bifunctional chelators (BFCs), consisting of an Aβ-affine aromatic moiety and a metal chelating scaffold, are widely used frameworks for designing of diagnostic agents for positron emission tomography (PET) Aβ plaques visualization.[17,18] Also, several studies have proven the therapeutic potential of such BFCs by demonstrating their ability to modulate amyloid aggregation, reduce amyloid toxicity, and oxidative stress.[8,19] Recently, we summarized the use of BFCs and coordination compounds based on them for AD therapy and imaging of AD hallmarks.[20]

Oxidative stress is one important consequence of metal ion dyshomeostasis.[21] In particular, the redox activity of the Cu(I/II) pair results in ROS overproduction from Fenton-like reactions.[22,23] Given the multifactorial etymology of AD, the design of several-targeted drugs is of high interest. Drugs capable of simultaneously interacting with several pathological components have been suggested as a solution to address the complex pathologies of neurodegenerative diseases.[24] Thus, imparting antioxidant or metal-binding functions to drugs that are clinically available is also on demand.[25,26]

Received: April 2, 2024
Revised: October 4, 2024
Accepted: October 9, 2024
Published: October 17, 2024

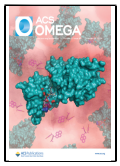

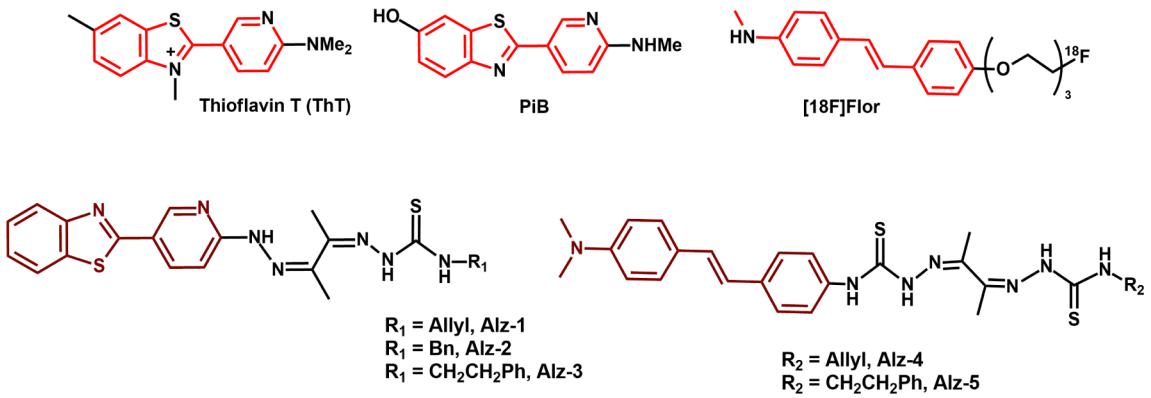

Figure 1. Structures of thioflavin-T, Pittsburgh compound B, ^{18}F − florbetaben, and bifunctional compounds **Alz-1**-**Alz-5**.

Table 1. Cell Viability Data of Alz-1−Alz-5 on HepG2 (Hepatocellular Carcinoma) and SH-SY5Y (Neuroblastoma) Cell Lines in the Presence and Absence of Copper Chloride (1:1)

	IC_{50}, μM										
Cells /Compounds	$CuCl_2$	Alz-1	Alz-1 + $CuCl_2$	Alz-2	Alz-2 + $CuCl_2$	Alz-3	Alz-3 + $CuCl_2$	Alz-4	Alz-4 + $CuCl_2$	Alz-5	Alz-5 + $CuCl_2$
HepG2	Nontoxic	Nontoxic	5.6 ± 0.9	Nontoxic	6.4 ± 1.6	Nontoxic	3.9 ± 0.8	Nontoxic	3.0 ± 1.0	Nontoxic	31.2 ± 9.7
SH-SY5Y	Nontoxic	Nontoxic	5.3 ± 1.0	Nontoxic	2.0 ± 0.4	Nontoxic	1.7 ± 0.6	Nontoxic	15.6 ± 1.8	Nontoxic	65.5 ± 15.1

RESULTS AND DISCUSSION

Herein, we report a synthesis investigation of five bifunctional copper chelators capable of disrupting metal-Aβ interactions based on benzothiazole and stilbene moieties. These well-known scaffolds originated from Pittsburgh compound B (PiB), a radioactive analogue of the Aβ staining agent thioflavin T(ThT), which is used for Aβ plaque imaging, and the ^{18}F-labeled stilbene derivative Florbetaben, which is also a PET radiotracer for Aβ-amyloid imaging.[27]

As copper-chelating scaffolds, thiocarbahydrazone and thiosemicarbazone moieties were used, which have also been successfully utilized in the design of amyloid-imaging drugs, as well as Cu-ATSM drugs.[28] Thiosemicarbazone derivatives have been extensively used as copper(II) chelators, as well as efficient antiaggregating agents.[29−32] The choice of allyl, benzyl, and phenylethyl moieties in molecular design was guided by our early studies on the antitumor activity of copper-containing coordination compounds (Figure 1).[33,34]

BFCs based on a benzothiazole scaffold with thiocarbahydrazone chelating moieties (**Alz-1−Alz-3**) were synthesized in six steps (Scheme S1), while BFCs based on a stilbene scaffold with thiosemicarbazone chelating moieties (**Alz-4, Alz-5**) were synthesized in nine steps (Scheme S2). The ligands were characterized by NMR, high resolution mass spectrometry, and IR, and the purity of **Alz-1 to Alz-5** was confirmed by HPLC (Figures S1, S38).

Since BFCs are intended to act as copper-chelating agents, their cell toxicity in the presence of copper cations should not be significant. Thus, the toxicity of the drugs on cancer-derived liver (HepG2) and neuronal (SH-SY5Y) cells was assessed. Based on the results (Table 1 and Figures S39, S40), **Alz-5** was the least toxic compound.

Cu-Alz-5 is a complex from the Cu-ATSM family, which are known to be stable neutral complexes with dissociation constants ~$K_d = 10^{-18}$.[35] It should also be noted, that **Alz-5** is deprotonated during the complexation process, according to the reaction $LH_2 + Cu^{2+} = CuL$. In the resulting **Cu-Alz-5** neutral complex, Cu^{2+} is coordinated to a dianionic tetradentate ligand.[36] In strict notation, the resulting complex corresponds to **Cu-[Alz-5−2H]**, but for simplicity, we refer to it as **Cu-Alz-5**. To estimate the dissociation constant, we used the method reported previously by

Donnelly et al. for a similar copper radiopharmaceutical capable of Aβ binding.[18] Thus, a competition binding assay for **Cu-Alz-5** with EDTA was performed using UV−vis titration (Figures S41, S42). The calculated K_d values were found to be 3.2×10^{-16} at pH = 7.4 and 6.3×10^{-14}, which are quite similar to those obtained by Donnelly et al.[18]

K_d values for Cu-Aβ complexes are reported to be 10^{-7}−10^{-10}, depending on experimental conditions.[37] As the K_d value obtained for **Cu-Alz-5** was 3.2×10^{-16} at pH = 7.4, **Alz-5** would be able to chelate copper ions from Cu-Aβ complex.

The Aβ binding affinity of **Alz-5** was assessed using fluorescence measurements. Aβ staining with ThT and **Alz-5** in the presence and absence of Cu^{2+} showed the ability of **Alz-5** to reduce the ThT emission intensity due to competitive binding to Aβ fibrils (Figure S43).

It is well-known that the formation of Aβ aggregates is accompanied by a disruption in mitochondrial activity and changes in the level of ROS, which causes multifaceted toxicity.[38] Thus, drugs that specifically scavenge oxygen radicals may have particular therapeutic efficacy.[38] The ability of **Alz-5** to reduce oxidative stress caused by the presence of Aβ amyloids was of extreme interest. To assess intracellular ROS level, single-cell amperometric ROS measurements using Pt-nanoelectrodes was used.[39,40]

The main advantage of in-cell electrochemical measurements is accurate single-cell analysis, allowing us to consistently measure the level of ROS in intact cells to which $A\beta_{42}$, the metal-chelating drug **Alz-5**, or both $A\beta_{42}$ and **Alz-5** have been added. Thus, the effect of $A\beta_{42}$, **Alz-5** or both on the intracellular ROS levels in single SH-SY5Y cells was assessed (Figure 2). As can be seen from the data obtained, the intracellular level of ROS increased by 2.2 times after incubation of SH-SY5Y cells with $A\beta_{42}$ for 4 h. Thus, the

https://doi.org/10.1021/acsomega.4c03152
ACS Omega 2024, 9, 43376−43384

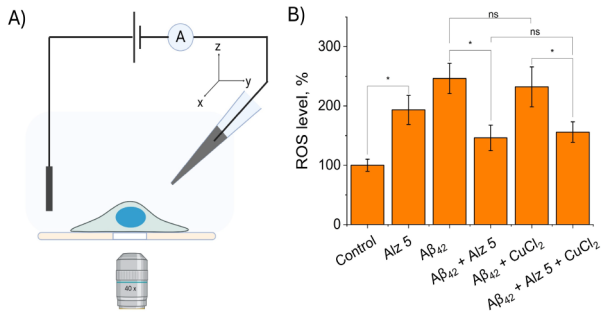

Figure 2. Electrochemical intracellular ROS measurement. (A) Scheme of measurement. (B) The ROS levels inside SH-SY5Y cells after incubation with Aβ_{42}, Alz 5, $CuCl_2$, or both. The average ROS level in control cells was 1.2 ± 0.2 μM. Results are shown as mean, SE, and (*) $p < 0.05$ (one-way ANOVA).

toxic effect of Aβ_{42} which results in ROS formation and oxidative stress was observed.

Then, we attempted to evaluate the role of **Alz-5** in reducing ROS levels in Aβ_{42}-affected SH-SY5Y cells. Previously, Sun et al. reported an amphiphilic BFC with the antioxidant activity, which was confirmed by ascorbate consumption assays.[41] Even though the addition of **Alz-5** to cells caused an increase in intracellular ROS levels, simultaneous incubation of Aβ_{42} with **Alz-5** led to a 1.7-fold decrease in intracellular ROS levels compared to Aβ_{42}. Statistically insignificant differences in the level of ROS were obtained in tested groups with the presence of Cu^{2+}. Thus, an antioxidant activity of **Alz-5** and its ability to reduce Aβ-induced oxidative stress were confirmed. Herein is the first example of real-time in-cell monitoring of Aβ- induced oxidative stress reduction, caused by a bifunctional copper chelator.

Atomic force microscopy (AFM) imaging technique is one of the best methods to assess drug-induced physiomechanical

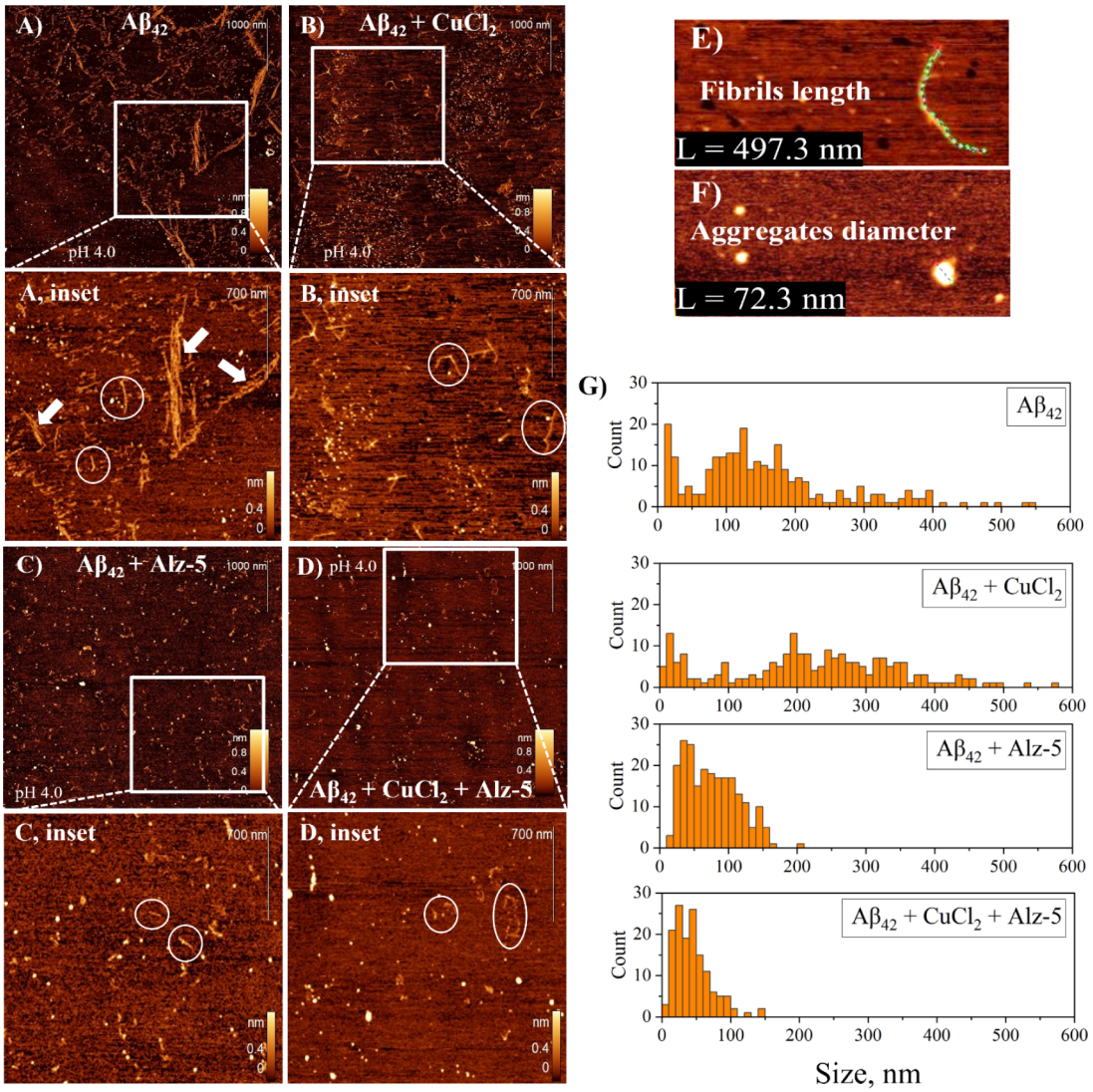

Figure 3. AFM imaging of diverse Aβ_{42} assemblies with histograms of distribution by size. AFM images of Aβ_{42} fibrils (A); Aβ_{42} + $CuCl_2$ (B); Aβ_{42} + **Alz-5**(C); and Aβ_{42} + $CuCl_2$ + **Alz-5**(D). Concentrations for all substances were 100 μM. All solutions were carefully resuspended and incubated at 37 °C for 24 h at pH 4.0. White squares indicate the enlarged areas in the insets (A–D), white circles in insets indicate the structures of aggregates that were used for statistical measurements, white arrows in the inset A indicates fibrils agglomerates. Examples of measured fibril length (F) and aggregate diameter (G). Histogram of Aβ_{42} aggregate sizes (fibrils and oligomers, N(Aβ_{42}) = 214, N(Aβ_{42}+$CuCl_2$) = 217, N(Aβ_{42}+**Alz-5**) = 223, N(Aβ_{42}+$CuCl_2$ + **Alz-5**) = 83) (E).

https://doi.org/10.1021/acsomega.4c03152
ACS Omega 2024, 9, 43376−43384

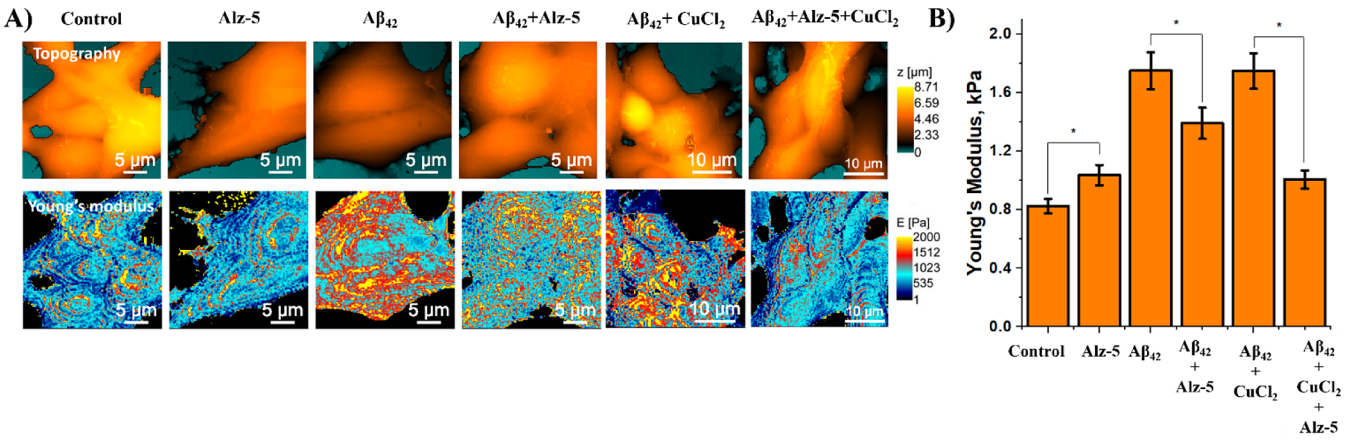

Figure 4. Topography and Young's modulus maps of control SH-SY5Y cells, after incubation with **Alz-5**, Aβ_{42}, Aβ_{42} + **Alz-5** and in the presence of $CuCl_2$(A); (B) Mean value of Young's modulus (*$p \leq 0.01$, one-way ANOVA) (B).

changes in amyloids.[42] Thus, the ability of **Alz-5** to modulate amyloid disaggregation was observed with AFM. Incubation of all samples of Aβ_{42} with complexes for AFM was performed at pH 4.0. The aggregation of Aβ_{42} for 24 h at 37 °C leads to the formation of well-defined Aβ_{42} fibrils up to 300 nm in length (Figure 3, A inset, marked with white circles), oligomeric aggregates, and large agglomerates up to 1.5 μm, consisting of many fibrils (Figure 3, A inset, marked with white arrows). It is important to note that we measured the length of the fibrils within the large agglomerate and did not measure the agglomerate as a whole. After $CuCl_2$ addition, large agglomerates were not observed, and the number of aggregates (long fibrils, protofibrils, and round oligomers) was significantly less compared to the control sample. However, fibril aggregation occurred up to 400 nm; i.e., fibril elongation was observed (Figure 3B inset, marked with white circles, Figure 3G). Thus, our AFM results on the incubation of Aβ_{42} with copper ions are consistent with a number of works using similar experimental conditions, namely the type of amyloid, equimolar or subequimolar peptide:metal ratio, acidic pH, and ionic strength of the solution.[43,44] The influence of internal and external conditions on the interaction of amyloid with metal ions is widely reviewed.[45] The addition of **Alz-5** leads to a shortening of aggregate size, up to ∼150 nm, along with reduced aggregation (Figure 3C). At the same time, in the presence of both copper chloride and **Alz-5**, oligomeric aggregates and structures, similar to protofibrils (Figure 3D inset, marked with white circles), were detected. Dimensions for fibrils were measured along their length, as shown in the example in Figure 3E; nonfibrillar aggregates (round oligomers) were measured along their diamete,r as shown in Figure 3F. Summarized data on aggregate length and diameter estimated using AFM are presented in Figure 3G. Thus, AFM data clearly indicate the antiaggregating properties of **Alz-5,** both in the absence and presence of Cu^{2+}. Also, denaturing SDS-PAGE followed by Western blotting confirmed that, in the presence of **Alz-5**, the proportion of monomers and low-molecular-weight oligomers in Aβ_{42} preparations (at pH 4.0) is higher than that in preparations without **Alz-5** (Figure S45). Moreover, the most significant differences are shown in the preparations with Cu^{2+}.

Scanning ion-conductance microscopy (SICM) is a unique method for studying living cells due to its use of noncontact probing and minimal deformation of the probe surface.[46] Measuring mechanical properties of cells is a unique technique for qualitative and quantitative drug efficacy screening, since it allows real-time detection of the cell response to the drug.[47] Amyloid fibrils have been repeatedly reported to cause cytoskeleton modifications, such as microtubule disassembly or actin polymerization, which results in degeneration of neurons.[48] The presence of amyloids in neuronal cells can lead to structural reorganization, a significant increase in fibrillar actin leads to increased cellular rigidity, which can be estimated using the SICM technique.[49,50] Recently, we reported the unique advantages of SICM for studying Aβ aggregate formation on living cell membranes, visualization of Aβ aggregates on live cells, and Young's modulus alteration.[51] Herein, we provide the first example of assessing the effect of a copper chelating agent on cell stiffness, administered using SICM. Thus, to evaluate the effect of **Alz-5** on the stiffness of a neuronal cell exposed to Aβ_{42}, we provided Young's modulus mapping of Aβ_{42} aggregates formation on the cell surface of living SH-SY5Y cell after incubation with **Alz-5** only, Aβ_{42}, and Aβ_{42} + **Alz-5,** as well as in the presence of $CuCl_2$. (Figure 4A).

As expected, the addition of Aβ_{42} to SH-SY5Y cells resulted in a dramatic increase in cell stiffness, which was inhibited by the addition of **Alz-5**. The decrease in Young's modulus can be explained by the inhibition of aggregation of beta-amyloid, which occurs even in the absence of copper cations. Summarized data on Young's modulus values estimated using SICM are presented in Figure 4B. Despite the incubation of SH-SY5Y cells with **Alz-5** alone led to an increase in Young's modulus compared to control cells, the obvious drop in cell rigidity caused by Aβ_{42} after **Alz-5** leaves no doubt about the effectiveness of **Alz-5** as an antiaggregating agent that acts even in the absence of copper cations. The addition of copper chloride to amyloids does not significantly increase cell stiffness; however, the addition of **Alz-5** to the SH-SY5Y cell-amyloid-copper chloride system leads to a significant decrease in Young's modulus, which indicates chelation of copper cations by **Alz-5** and disaggregation of amyloids.

■ CONCLUSIONS

Herein, we report the design and synthesis of BFCs Alz-**1** through Alz-**5**, which are capable of Aβ_{42} binding and chelating metals. **Alz-5** showed a promising ability to modulate the aggregation of Aβ in the presence of copper cations. Single-cell ROS measurements using the Pt-nanoelectrode technique

https://doi.org/10.1021/acsomega.4c03152
ACS Omega 2024, 9, 43376−43384

revealed a significant Aβ_{42}-induced oxidative stress reduction in the presence of **Alz-5**. AFM data obtained on Aβ_{42} fibrils clearly indicate the antiaggregating properties of **Alz-5**, both in the presence and absence of Cu^{2+}. Young's modulus mapping and confocal imaging of Aβ_{42} aggregate formation on living SH-SY5Y cells revealed a decrease in Aβ_{42}-affected SH-SY5Y cell rigidity.

METHODS

Synthesis. Synthetic procedures and characterization are provided in SI.

Stability Constants Determination. The stability constant of **Alz-5** was estimated using a competitive ligand binding assay with Na_2H_2EDTA. An equimolar PBS solution of equimolar amounts of Alz-5 and copper chloride (20 μM, 30% DMSO, pH 7.4 or 6.5) was incubated with EDTA for 24 h at room temperature. Five UV−vis spectra were collected with different ratios of Alz-5-Cu and EDTA. The stability constant for the Cu-Alz-5 complex was determined by fitting the observed absorbance data at 320 nm according to the following equation:

$$\text{Cu-Alz-5} + \text{EDTA} \leftrightarrow \text{Alz-5} + \text{Cu-EDTA}$$

$$y = \frac{K \times x}{C(1 - x)} + x$$

where y = [Cu-Alz-5]/[EDTA], x = saturation fraction = $(A_L - A_O)/(A_L - A_C)$, where A_L, A_O, and A_C are absorption values in the absence of EDTA, in the presence of EDTA, and at saturation of EDTA respectively, C is the total concentration of ligand, and K is the equilibrium constant. Thus, stability constant can be estimated by Cu-EDTA stability constant ($K_d = 1.10 \times 10^{-16}$ at pH = 7.4 and $K_d = 7.88 \times 10^{-14}$ at pH = 6.5).

$$\text{Kd}(\text{Cu} - \text{Alz} - 5) = \text{Kd}(\text{Cu} - \text{EDTA}) \times K$$

Amyloid Preparation. A preparation of synthetic peptide of 42 amino acids β-amyloid Aβ_{42} (PepMic, China) was carried out using standard technology.[52] For this, 1 mg of the powder was dissolved in 1,1,1,3,3,3-hexafluoro-2-propanol (Sigma, USA) on ice to reach a final peptide concentration of 1 mM in a glass vial. After dissolution, the solution was incubated 1 h at room temperature to obtain peptide monomers. Then, the vial with the peptide was placed back on ice for 5−10 min, and the resulting solution was aliquoted into microtubes. Next, the tubes were left open to allow for evaporation of 1,1,1,3,3,3-hexafluoro-2-propanol. Any remaining alcohol was evaporated using a rotary evaporator for 1 h, and the resulting films were stored at −70 °C. For Western blot assay, Aβ_{42} samples were prepared in accordance with the incubation protocol used for AFM. After the 24 h incubation, acidic Aβ_{42} solutions were neutralized with NaOH to achieve a pH of 6.5 directly before the analysis. A solution of Aβ_{42} monomers was used as a control (100 μM in PBS 1× pH 4.0, neutralized with NaOH).

Cytotoxicity Assay. For the study of the IC_{50} of substances and Cu-ions effect, a cytotoxicity assay was performed using HepG2 and SH-SY5Y cell lines (ATCC) along with the MTS reagent (Promega). The standard research protocol consisted of the following steps: 10000 cells were seeded in the wells of a 96-well plate in a DMEM/F12-based growth medium with 10% FBS, 2 mM L-glutamine, 100 units/mL penicillium, 100 units/mL streptomycin. After 24 h of incubation at 37 °C and 5% CO_2, the growth medium was replaced with a medium containing the test substances at concentrations from 0.4 to 100 μM (with DMSO content 0.1 5 and less), with and without $CuCl_2$ in the same concentrations, and incubated for 48 h. Dose−response curves are provided in SI.

Fluorescence Measurements. All fluorescence measurements were performed by using a Varioskan LUX plate reader (Thermo Scientific). A stock solution of β-amyloid peptide in DMSO (1.25 mM) was dissolved in filtered PBS 1× (pH 4.0) to a final concentration of 100 μM. Incubation at acidic pH accelerates the aggregation process, which improves the fluorescence intensity of the fibril-specific thioflavin T dye. Four solutions were prepared as follows: 1. first solution was used as a control sample (Aβ_{42}); 2. 100 μM Aβ_{42} + 100 μM $CuCl_2$ (Aβ_{42} + $CuCl_2$); 3. 100 μM Aβ_{42} + 100 μM **Alz-5** (Aβ_{42} + **Alz-5**); 4. 100 μM Aβ_{42} + 100 μM $CuCl_2$ + 100 μM **Alz-5** (Aβ_{42} + $CuCl_2$ + **Alz-5**). All solutions were carefully resuspended and incubated at 37 °C for 24 h. After incubation time, the solutions were thoroughly mixed by vortexing. A 96-well plate was used for fluorescence measurements, with 100 μL of each sample added into a plate, including the four amyloid solutions, $CuCl_2$, **Alz-5**,and $CuCl_2$ + **Alz-5** controls. Since ThT fluoresces poorly at low pH, directly before adding 100 μM ThT, samples were alkalized with PBS (pH 7.4) to pH ∼ 6. The final concentration of each reagent in the plate was 100 μM. Fluorescence (λex/λem = 440/480 nm) and fluorescence emission spectrum (λex = 440 nm, emission range of 460−550 nm) were measured. The fluorescence spectra were analyzed and plotted using OriginPro.

Amperometric ROS Measurements. The total ROS concentration was determined by an amperometric method using Pt-nanoelectrodes. Commercially available disk-shaped carbon nanoelectrodes isolated in quartz (ICAPPIC Limited, UK), with diameters 60−100 nm, were used to prepare Pt nanoelectrodes. First, the carbon surface was etched in a 0.1 M NaOH, 10 mM KCl solution for 40 cycles of 10 seconds (from 0 to +2200 mV) to create nanocavities. Further electrochemical deposition of platinum in the nanocavities was achieved by cycling from 0 to 800 mV with a scan rate of 200 mV/s for 4 to 5 cycles in a 2 mM H_2PtCl_6 solution in 0.1 M hydrochloric acid. Cyclic voltammetry from −800 to 800 mV, with a scan rate of 400 mV/s in a 1 mM solution of ferrocene in methanol in PBS, was used to control the electrode surface at all stages of fabrication. Prior to the measurements, each platinum nanoelectrode was calibrated using a series of standard H_2O_2 solutions at a potential of +800 mV vs Ag/AgCl. The preparation of Pt-nanoelectrodes has been described in detail elsewhere.[39,53]

SH-SY5Y (3×10^5) cells were seeded in 35 mm Petri dishes and treated on the next day with Aβ_{42}/**Alz-5** or Aβ_{42} with **Alz-5** simultaneously. Aβ_{42} and **Alz-5** were dissolved in DMSO. The final concentrations of Aβ_{42}/$CuCl_2$/**Alz-5** in the culture medium were 10 μM (Aβ_{42}, $CuCl_2$)/50 μM (**Alz-5**) with 4 h of incubation time. Untreated cells were used as a control, which was performed at the beginning and end of the experiment. Before the experiment, the attached cells in the Petri dishes were washed three times using Hanks' Balanced Salt solution to remove the growth media and traces of Aβ_{42}/**Alz-5**. A nanoelectrode penetrated the cells and measured the oxidation current of hydrogen peroxide. On average, about 15 cells were measured using 2−3 Pt electrodes in independent Petri dishes.

The setup for amperometric measurements included a PC that was connected to a system consisting of an ADC-DAC

https://doi.org/10.1021/acsomega.4c03152
ACS Omega 2024, 9, 43376−43384

converter, Axon Digidata 1550B (Axon Instruments, USA) and a patch-clamp amplifier, MultiClamp 700B (Axon Instruments, USA). The working head of the amplifier was fixed to a PatchStar Micromanipulator (Scientifica, UK), which was placed near an inverted optical microscope Nikon Eclipse TI-U (Nikon, Japan). A Pt nanoelectrode was fixed by a special holder on the working head of the amplifier. The potential difference between the Pt nanoelectrode and the reference (Ag/AgCl) electrode was recorded with the pClamp 11 software suite (Molecular Devices, USA) and processed with Origin 2018 software.

Scanning Ion-Conductance Microscopy (SICM). SICM by ICAPPIC (ICAPPIC ltd, United Kingdom) was used for topography mapping and estimation of Young's modulus of SH-SY5Y cells. Nanopipettes with a typical tip radius of 45−50 nm were fabricated from borosilicate glass O.D. 1.0 mm, I.D. 0.5 mm (WPI, United Kingdom) using a laser puller *p*-2000 (Sutter Instruments, USA). Nanopipette radius was calculated using by following theoretical model:[54]

$$r = \frac{Io}{\pi Vktg(\alpha)}$$

where the half-cone angle α is 3 degrees, κ is 1.35 S m^{-1}, and V is the applied electrical potential of 200 mV.

The scanning procedure was performed in Hank's solution (Gibco, USA). Each experimental pointinvolved scanning 20−30 cells. For estimating Young's modulus of living cells, a nanopipette was approached to the surface until the ion current through the tip reduced by 2% from its initial value during scanning.[43] A noncontact topographic image was obtained at an ion current decreases of 0.5%, and further two images were obtained at an ion current decreases (or set points) of 1% and 2%, corresponding to membrane deformations produced by intrinsic force at each set point. Then, Young's modulus estimated using the following model:

$$E = PA\left(\frac{Ssub}{Scell} - 1\right)^{-1}$$

where E is the estimated Young's modulus, P is the applied pressure, A is a constant depending on the nanopipette geometry, and S_{sub} and S_{cell} are the slopes of the current−distance curve observed between the ion current decreases of 1% and 2% at the nondeformable surface (S_{sub} − substrate) and cell surface (S_{cell}), respectively.

Atomic-Force Microscopy (AFM). A stock solution of β-amyloid peptide in DMSO (1.25 mM) was dissolved in filtered PBS 1× pH 4.0 to a final concentration of 100 μM. Incubation at acidic pH accelerates the aggregation process of amyloid peptides into fibrils [10.1074/jbc.M210207200, 10.1002/anie.202210675], which improves AFM analysis. Since fibrils are clearly visible via AFM, the effect of **Alz-5** on the aggregation of monomers incubated under the same conditions could be recognized. Four solutions were prepared as follows: 1. the first solution was used as a control sample ($A\beta_{42}$); 2. 100 μM $A\beta_{42}$ + 100 μM $CuCl_2$ ($A\beta_{42}$ + $CuCl_2$); 3. 100 μM $A\beta_{42}$ + 100 μM **Alz-5** ($A\beta_{42}$ + **Alz-5**); 4. 100 μM $A\beta_{42}$ + 100 μM $CuCl_2$ + 100 μM **Alz-5** ($A\beta_{42}$ + $CuCl_2$ + **Alz-5**). All solutions were carefully resuspended and incubated at 37 °C for 24 h. After the incubation time, the solutions were thoroughly mixed by vortexing and diluted with ultrapure water 10 times to a final concentration of $A\beta_{42}$ of 10 μM. For atomic force microscopy scans, 10 μL of each sample was placed on freshly cleaved mica and incubated in a Petri dish for 10 min for peptide adsorption onto the mica. After the adsorption time, the mica samples were washed with 1 mL of ultrapure water and dried in an argon flow. AFM scans were carried out on an NTEGRA II microscope (NT-MDT SI, Russia) in semicontact mode with silicon cantilevers (1.74 N/m, 90 kHz), scan rates 0.5−0.8 Hz, oscillation amplitude is 20 nm, gain values of 0.5−0.7, a scan size of 1−5 μm, and 512 points. AFM images were processed in Femtoscan software (Advanced Technologies Center, Russia).[55] For the statistical analysis of aggregates size, the length and diameter of the aggregates were traced manually from the images by linear segments using the special tool in the software (Figure S44). For each sample 2−4 images were used, and total number of measured aggregates for each sample from the corresponding images was as follows: N($A\beta_{42}$) = 214, N($A\beta_{42}$+$CuCl_2$) = 217, N($A\beta_{42}$+Alz-5) = 223, and N-($A\beta_{42}$+$CuCl_2$ + Alz-5) = 83. The selected contours were converted into sequences of two-dimensional coordinates and the obtained data were presented in the form of histograms with bin size 10.

■ ASSOCIATED CONTENT

Supporting Information

The Supporting Information is available free of charge at https://pubs.acs.org/doi/10.1021/acsomega.4c03152.

Synthetic procedures, characterization of the compounds, dose−response curves (PDF)

■ AUTHOR INFORMATION

Corresponding Authors

Olga Krasnovskaya − *Chemistry Department, Lomonosov Moscow State University, Moscow 119991, Russia;* orcid.org/0000-0002-4948-2747; Email: Krasnovskayao@gmail.com

Alexander Erofeev − *Chemistry Department, Lomonosov Moscow State University, Moscow 119991, Russia; National University of Science and Technology (MISIS), Moscow 119049, Russia*; Email: Erofeev@polly.phys.msu.ru

Authors

Daniil Abramchuk − *Chemistry Department, Lomonosov Moscow State University, Moscow 119991, Russia*

Alexander Vaneev − *Chemistry Department, Lomonosov Moscow State University, Moscow 119991, Russia; National University of Science and Technology (MISIS), Moscow 119049, Russia;* orcid.org/0000-0001-8201-8498

Petr Gorelkin − *National University of Science and Technology (MISIS), Moscow 119049, Russia*

Maxim Abakumov − *National University of Science and Technology (MISIS), Moscow 119049, Russia; Pirogov Russian National Research Medical University (RNRMU), Moscow 117997, Russia;* orcid.org/0000-0003-2622-9201

Roman Timoshenko − *National University of Science and Technology (MISIS), Moscow 119049, Russia;* orcid.org/0009-0007-6459-6455

Ilia Kuzmichev − *Serbsky National Medical Research Center for Psychiatry and Narcology, Moscow 119991, Russia;* orcid.org/0009-0004-7092-1777

Nelly Chmelyuk − *National University of Science and Technology (MISIS), Moscow 119049, Russia;* orcid.org/0000-0002-2434-2465

https://doi.org/10.1021/acsomega.4c03152
ACS Omega 2024, 9, 43376−43384

Veronika Vadehina − *Pirogov Russian National Research Medical University (RNRMU), Moscow 117997, Russia; Serbsky National Medical Research Center for Psychiatry and Narcology, Moscow 119991, Russia*
Regina Kuanaeva − *National University of Science and Technology (MISIS), Moscow 119049, Russia*
Evgeniy Dubrovin − *National University of Science and Technology (MISIS), Moscow 119049, Russia; Faculty of Physics, Lomonosov Moscow State University, Moscow 119991, Russia;* orcid.org/0000-0001-8883-5966
Vasilii Kolmogorov − *National University of Science and Technology (MISIS), Moscow 119049, Russia;* orcid.org/0000-0002-7135-8910
Elena Beloglazkina − *Chemistry Department, Lomonosov Moscow State University, Moscow 119991, Russia;* orcid.org/0000-0001-6796-8241
Olga Kechko − *Engelhardt Institute of Molecular Biology, Russian Academy of Sciences, Moscow 119991, Russia*
Vladimir Mitkevich − *Engelhardt Institute of Molecular Biology, Russian Academy of Sciences, Moscow 119991, Russia*
Kseniya Varshavskaya − *Engelhardt Institute of Molecular Biology, Russian Academy of Sciences, Moscow 119991, Russia*
Sergey Salikhov − *National University of Science and Technology (MISIS), Moscow 119049, Russia*

Complete contact information is available at: https://pubs.acs.org/10.1021/acsomega.4c03152

Author Contributions

The manuscript was written through contributions of all authors.

Funding

The study was performed employing a unique scientific facility "Scanning ion-conductance microscope with a confocal module" (registration number 2512 530) and was financially supported by the Ministry of Science and Higher Education of the Russian Federation, Agreement No. 075−15−2022−264.

Notes

The authors declare no competing financial interest.

■ ABBREVIATIONS

(SICM) scanning ion-conductance microscopy
(ROS) reactive oxygen species
(BFCs) bifunctional chelators
(AD) Alzheimer's disease
(AFM) atomic force microscopy.

■ REFERENCES

(1) Bloom, G. S. Amyloid-β and tau: the trigger and bullet in Alzheimer disease pathogenesis. *JAMA Neurol.* **2014**, *71* (4), 505−508.
(2) Butterfield, D. A.; Halliwell, B. Oxidative stress, dysfunctional glucose metabolism and Alzheimer disease. *Nat. Rev. Neurosci.* **2019**, *20* (3), 148−160.
(3) Calsolaro, V.; Edison, P. Neuroinflammation in Alzheimer's disease: Current evidence and future directions. *Alzheimer's & Dementia* **2016**, *12* (6), 719−732.
(4) Nelson, P. T.; Braak, H.; Markesbery, W. R. Neuropathology and cognitive impairment in Alzheimer disease: a complex but coherent relationship. *J. Neuropathol. Exper. Neurol.* **2009**, *68* (1), 1−4.
(5) Miller, L. M.; Wang, Q.; Telivala, T. P.; Smith, R. J.; Lanzirotti, A.; Miklossy, J. Synchrotron-based infrared and X-ray imaging shows focalized accumulation of Cu and Zn co-localized with β-amyloid deposits in Alzheimer's disease. *J. Struct. Biol.* **2006**, *155* (1), 30−37.
(6) Chen, L. L.; Fan, Y. G.; Zhao, L. X.; Zhang, Q.; Wang, Z. Y. The metal ion hypothesis of Alzheimer's disease and the anti-neuroinflammatory effect of metal chelators. *Bioorg. Chem.* **2023**, *131*, 106301.
(7) Li, Y.; Jiao, Q.; Xu, H.; Du, X.; Shi, L.; Jia, F.; Jiang, H. Biometal dyshomeostasis and toxic metal accumulations in the development of Alzheimer's disease. *Front. Mol. Neurosci.* **2017**, *10*, 339.
(8) Kepp, K. P. Bioinorganic chemistry of Alzheimer's disease. *Chem. Rev.* **2012**, *112* (10), 5193−5239.
(9) Faller, P.; Hureau, C.; La Penna, G. Metal ions and intrinsically disordered proteins and peptides: from Cu/Zn amyloid-β to general principles. *Acc. Chem. Res.* **2014**, *47* (8), 2252−2259.
(10) Kepp, K. P. Alzheimer's disease: How metal ions define β-amyloid function. *Coord. Chem. Rev.* **2017**, *351*, 127−159.
(11) Puentes-Díaz, N.; Chaparro, D.; Morales-Morales, D.; Flores-Gaspar, A.; Alí-Torres, J. Role of metal cations of copper, Iron, and aluminum and multifunctional ligands in Alzheimer's disease: Experimental and computational insights. *ACS Omega* **2023**, *8* (5), 4508−4526.
(12) Atwood, C. S.; Scarpa, R. C.; Huang, X.; Moir, R. D.; Jones, W. D.; Fairlie, D. P.; Tanzi, R. E.; Bush, A. I. Characterization of copper interactions with Alzheimer amyloid β peptides: identification of an attomolar-affinity copper binding site on amyloid β1−42. *J. Neurochem.* **2000**, *75* (3), 1219−1233.
(13) Abelein, A. Metal Binding of Alzheimer's Amyloid-β and Its Effect on Peptide Self-Assembly. *Acc. Chem. Res.* **2023**, *56* (19), 2653−2663.
(14) Parthasarathy, S.; Long, F.; Miller, Y.; Xiao, Y.; McElheny, D.; Thurber, K.; Ma, B.; Nussinov, R.; Ishii, Y. Molecular-level examination of Cu2+ binding structure for amyloid fibrils of 40-residue Alzheimer's β by solid-state NMR spectroscopy. *J. Am. Chem. Soc.* **2011**, *133* (10), 3390−3400.
(15) Liu, Y.; Nguyen, M.; Robert, A.; Meunier, B. Metal ions in Alzheimer's disease: a key role or not? *Acc. Chem. Res.* **2019**, *52* (7), 2026−2035.
(16) Hegde, M. L.; Bharathi, P.; Suram, A.; Venugopal, C.; Jagannathan, R.; Poddar, P.; Srinivas, P.; Sambamurti, K.; Rao, K. J.; Scancar, J.; Messori, L. Challenges associated with metal chelation therapy in Alzheimer's disease. *J. Alzheimer's Disease* **2009**, *17* (3), 457−468.
(17) Krasnovskaya, O.; Kononova, A.; Erofeev, A.; Gorelkin, P.; Majouga, A.; Beloglazkina, E. Aβ-targeting bifunctional chelators (BFCs) for potential therapeutic and PET imaging applications. *Int. J. Mol. Sci.* **2023**, *24* (1), 236.
(18) Hickey, J. L.; Lim, S.; Hayne, D. J.; Paterson, B. M.; White, J. M.; Villemagne, V. L.; Roselt, P.; Binns, D.; Cullinane, C.; Jeffery, C. M.; Price, R. I.; et al. Diagnostic imaging agents for Alzheimer's disease: copper radiopharmaceuticals that target Aβ plaques. *J. Am. Chem. Soc.* **2013**, *135* (43), 16120−16132.
(19) Sharma, A. K.; Pavlova, S. T.; Kim, J.; Finkelstein, D.; Hawco, N. J.; Rath, N. P.; Kim, J.; Mirica, L. M. Bifunctional compounds for controlling metal-mediated aggregation of the Aβ42 peptide. *J. Am. Chem. Soc.* **2012**, *134* (15), 6625−6636.
(20) Krasnovskaya, O.; Spector, D.; Zlobin, A.; Pavlov, K.; Gorelkin, P.; Erofeev, A.; Beloglazkina, E.; Majouga, A. Metals in Imaging of Alzheimer's Disease. *Int. J. Mol. Sci.* **2020**, *21* (23), 9190.
(21) Gomes, L. M.; Vieira, R. P.; Jones, M. R.; Wang, M. C.; Dyrager, C.; Souza-Fagundes, E. M.; Da Silva, J. G.; Storr, T.; Beraldo, H. 8-Hydroxyquinoline Schiff-base compounds as antioxidants and modulators of copper-mediated Aβ peptide aggregation. *J. Inorg. Biochem.* **2014**, *139*, 106−116.
(22) Greenough, M. A.; Camakaris, J.; Bush, A. I. Metal dyshomeostasis and oxidative stress in Alzheimer's disease. *Neurochem. Int.* **2013**, *62* (5), 540−555.
(23) Abelein, A.; Ciofi-Baffoni, S.; Mörman, C.; Kumar, R.; Giachetti, A.; Piccioli, M.; Biverstål, H. Molecular Structure of Cu (II)-Bound Amyloid-β Monomer Implicated in Inhibition of Peptide

Self-Assembly in Alzheimer's Disease. *JACS Au.* **2022**, *2* (11), 2571−2584.
(24) Savelieff, M. G.; Nam, G.; Kang, J.; Lee, H. J.; Lee, M.; Lim, M. H. Development of multifunctional molecules as potential therapeutic candidates for Alzheimer's disease, Parkinson's disease, and amyotrophic lateral sclerosis in the last decade. *Chem. Rev.* **2019**, *119* (2), 1221−1322.
(25) Sestito, S.; Wang, S.; Chen, Q.; Lu, J.; Bertini, S.; Pomelli, C.; Chiellini, G.; He, X.; Pi, R.; Rapposelli, S. Multi-targeted ChEI-copper chelating molecules as neuroprotective agents. *Eur. J. Med. Chem.* **2019**, *174*, 216−225.
(26) Bubley, A.; Erofeev, A.; Gorelkin, P.; Beloglazkina, E.; Majouga, A.; Krasnovskaya, O. Tacrine-Based Hybrids: Past, Present, and Future. *Int. J. Mol. Sci.* **2023**, *24* (2), 1717.
(27) Sabri, O.; Sabbagh, M. N.; Seibyl, J.; Barthel, H.; Akatsu, H.; Ouchi, Y.; Senda, K.; Murayama, S.; Ishii, K.; Takao, M.; Beach, T. G. Florbetaben PET imaging to detect amyloid beta plaques in Alzheimer's disease: Phase 3 study. *Alzheimer's & Dementia* **2015**, *11* (8), 964−974.
(28) Xie, F.; Wei, W. [64Cu] Cu-ATSM: an emerging theranostic agent for cancer and neuroinflammation. *European Eur. J. Nucl. Med. Mol. Imaging* **2022**, *49* (12), 3964−3972.
(29) D'Acunto, C. W.; Kaplánek, R.; Gbelcová, H.; Kejík, Z.; Bříza, T.; Vasina, L.; Havlík, M.; Ruml, T.; Král, V. Metallomics for Alzheimer's disease treatment: Use of new generation of chelators combining metal-cation binding and transport properties. *Eur. J. Med. Chem.* **2018**, *150*, 140−155.
(30) Ranade, D. S.; Shravage, B. V.; Kumbhar, A. A.; Sonawane, U. B.; Jani, V. P.; Joshi, R. R.; Kulkarni, P. P. Thiosemicarbazone moiety assist in interaction of planar aromatic molecules with amyloid beta peptide and acetylcholinesterase. *ChemistrySelect* **2017**, *2* (13), 3911−3916.
(31) Matesanz, A. I.; Caballero, A. B.; Lorenzo, C.; Espargaro, A.; Sabate, R.; Quiroga, A. G.; Gamez, P. Thiosemicarbazone derivatives as inhibitors of amyloid-β aggregation: Effect of metal coordination. *Inorg. Chem.* **2020**, *59* (10), 6978−6987.
(32) Palanimuthu, D.; Poon, R.; Sahni, S.; Anjum, R.; Hibbs, D.; Lin, H. Y.; Bernhardt, P. V.; Kalinowski, D. S.; Richardson, D. R. A novel class of thiosemicarbazones show multi-functional activity for the treatment of Alzheimer's disease. *Eur. J. Med. Chem.* **2017**, *139*, 612−632.
(33) Majouga, A. G.; Zvereva, M. I.; Rubtsova, M. P.; Skvortsov, D. A.; Mironov, A. V.; Azhibek, D. M.; Krasnovskaya, O. O.; Gerasimov, V. M.; Udina, A. V.; Vorozhtsov, N. I.; Beloglazkina, E. K.; et al. Mixed valence copper (I, II) binuclear complexes with unexpected structure: synthesis, biological properties and anticancer activity. *J. Med. Chem.* **2014**, *57* (14), 6252−6258.
(34) Beloglazkina, E. K.; Krasnovskaya, O. O.; Guk, D. A.; Tafeenko, V. A.; Moiseeva, A. A.; Zyk, N. V.; Majouga, A. G. Synthesis, characterization, and cytotoxicity of binuclear copper (II) complexes with tetradentate nitrogen-containing ligands bis-5-(2-pyridylmethylidene)-3, 5-dihydro-4H-imidazol-4-ones. *Polyhedron* **2018**, *148*, 129−137.
(35) Lum, J. S.; Brown, M. L.; Farrawell, N. E.; McAlary, L.; Ly, D.; Chisholm, C. G.; Snow, J.; Vine, K. L.; Karl, T.; Kreilaus, F.; McInnes, L. E.; et al. CuATSM improves motor function and extends survival but is not tolerated at a high dose in SOD1 G93A mice with a C57BL/6 background. *Sci. Rep.* **2021**, *11* (1), 19392.
(36) Beloglazkina, E. K.; Moiseeva, A. A.; Tsymbal, S. A.; Guk, D. A.; Kuzmin, M. A.; Krasnovskaya, O. O.; Borisov, R. S.; Barskaya, E. S.; Tafeenko, V. A.; Alpatova, V. M.; Zaitsev, A. V.; et al. The Copper Reduction Potential Determines the Reductive Cytotoxicity: Relevance to the Design of Metal−Organic Antitumor Drugs. *Molecules* **2024**, *29* (5), 1032.
(37) Zawisza, I.; Rózga, M.; Bal, W. Affinity of copper and zinc ions to proteins and peptides related to neurodegenerative conditions (Aβ, APP, α-synuclein, PrP). *Coord. Chem. Rev.* **2012**, *256* (19−20), 2297−2307.
(38) Sharma, A. K.; Pavlova, S. T.; Kim, J.; Kim, J.; Mirica, L. M. The effect of Cu2+ and Zn2+ on the Aβ42 peptide aggregation and cellular toxicity. *Metallomics* **2013**, *5* (11), 1529−1536.
(39) Savin, N.; Erofeev, A.; Timoshenko, B.; Vaneev, A.; Garanina, A.; Salikhov, S.; Grammatikova, N.; Levshin, I.; Korchev, Y.; Gorelkin, P. Investigation of the Antifungal and Anticancer Effects of the Novel Synthesized Thiazolidinedione by Ion-Conductance Microscopy. *Cells* **2023**, *12* (12), 1666.
(40) Vaneev, A. N.; Gorelkin, P. V.; Garanina, A. S.; Lopatukhina, H. V.; Vodopyanov, S. S.; Alova, A. V.; Ryabaya, O. O.; Akasov, R. A.; Zhang, Y.; Novak, P.; Salikhov, S. V. In vitro and in vivo electrochemical measurement of reactive oxygen species after treatment with anticancer drugs. *Anal. Chem.* **2020**, *92* (12), 8010−8014.
(41) Sun, L.; Cho, H. J.; Sen, S.; Arango, A. S.; Huynh, T. T.; Huang, Y.; Bandara, N.; Rogers, B. E.; Tajkhorshid, E.; Mirica, L. M. Amphiphilic distyrylbenzene derivatives as potential therapeutic and imaging agents for soluble and insoluble amyloid β aggregates in Alzheimer's disease. *J. Am. Chem. Soc.* **2021**, *143* (27), 10462−10476.
(42) Wang, X.; Bleher, R.; Brown, M.; Garcia, J. G. N.; Dudek, S. M.; Shekhawat, G. S.; Dravid, V. P. Nano-Biomechanical Study of Spatio-Temporal Cytoskeleton Rearrangements that Determine Subcellular Mechanical Properties and Endothelial Permeability. *Sci. Rep.* **2015**, *5* (1), 11097.
(43) Ha, C.; Ryu, J.; Park, C. B. Metal ions differentially influence the aggregation and deposition of Alzheimer's β-amyloid on a solid template. *Biochemistry* **2007**, *46* (20), 6118−6125.
(44) Lv, Z.; Condron, M. M.; Teplow, D. B.; Lyubchenko, Y. L. Nanoprobing of the Effect of Cu2+ Cations on Misfolding, Interaction and Aggregation of Amyloid beta Peptide. *Biophys. J.* **2013**, *104* (2), 513a−514a.
(45) Faller, P.; Hureau, C.; Berthoumieu, O. Role of metal ions in the self-assembly of the Alzheimer's amyloid-β peptide. *Inorg. Chem.* **2013**, *52* (21), 12193−12206.
(46) Zhang, Y.; Takahashi, Y.; Hong, S. P.; Liu, F.; Bednarska, J.; Goff, P. S.; Novak, P.; Shevchuk, A.; Gopal, S.; Barozzi, I.; Magnani, L. High-resolution label-free 3D mapping of extracellular pH of single living cells. *Nat. Commun.* **2019**, *10* (1), 5610.
(47) Kolmogorov, V. S.; Erofeev, A. S.; Woodcock, E.; Efremov, Y. M.; Iakovlev, A. P.; Savin, N. A.; Alova, A. V.; Lavrushkina, S. V.; Kireev, I. I.; Prelovskaya, A. O. Mapping mechanical properties of living cells at nanoscale using intrinsic nanopipette−sample force interactions. *Nanoscale* **2021**, *13*, 6558−6568.
(48) Ungureanu, A.-A.; Benilova, I.; Krylychkina, O.; Braeken, D.; De Strooper, B.; Van Haesendonck, C.; Dotti, C. G.; Bartic, C. Amyloid beta oligomers induce neuronal elasticity changes in age-dependent manner: a force spectroscopy study on living hippocampal neurons. *Sci. Rep.* **2016**, *6* (1), 25841.
(49) Lopez, M.; Aguilera, R.; Perez, C.; Mendoza-Naranjo, A.; Pereda, C.; Ramirez, M.; Ferrada, C.; Aguillon, J. C.; Salazar-Onfray, F. The role of regulatory T lymphocytes in the induced immune response mediated by biological vaccines. *Immunobiology* **2006**, *211* (1−2), 127−136.
(50) Suchalko, O.; Timoshenko, R.; Vaneev, A.; Kolmogorov, V.; Savin, N.; Klyachko, N.; Barykin, E.; Gorbacheva, L.; Maksimov, G.; Kozin, S.; Erofeev, A. Cell stiffness and ROS level alterations in living neurons mediated by β-amyloid oligomers measured by scanning ion-conductance microscopy. *Microsc. Microanal.* **2021**, *27* (S1), 500−502.
(51) Kolmogorov, V. S.; Erofeev, A. S.; Barykin, E. P.; Timoshenko, R. V.; Lopatukhina, E. V.; Kozin, S. A.; Gorbacheva, L. R.; Salikhov, S. V.; Klyachko, N. L.; Mitkevich, V. A. Scanning Ion-Conductance Microscopy for Studying β-Amyloid Aggregate Formation on Living Cell Surfaces. *Anal. Chem.* **2023**, *95*, 15943−15949.
(52) Zatsepina, O. G.; Kechko, O. I.; Mitkevich, V. A.; Kozin, S. A.; Yurinskaya, M. M.; Vinokurov, M. G.; Serebryakova, M. V.; Rezvykh, A. P.; Evgen'ev, M. B.; Makarov, A. A. Amyloid-β with isomerized Asp7 cytotoxicity is coupled to protein phosphorylation. *Sci. Rep.* **2018**, *8* (1), 3518.

https://doi.org/10.1021/acsomega.4c03152
ACS Omega 2024, 9, 43376−43384

(53) Erofeev, A.; Gorelkin, P.; Garanina, A.; Alova, A.; Efremova, M.; Vorobyeva, N.; Edwards, C.; Korchev, Y.; Majouga, A. Novel method for rapid toxicity screening of magnetic nanoparticles. *Sci. Rep.* **2018**, *8* (1), 7462.
(54) Clarke, R. W.; Novak, P.; Zhukov, A.; Tyler, E. J.; Cano-Jaimez, M.; Drews, A.; Richards, O.; Volynski, K.; Bishop, C.; Klenerman, D. Low stress ion conductance microscopy of sub-cellular stiffness. *Soft Matter* **2016**, *12* (38), 7953−7958.
(55) Yaminsky, I.; Akhmetova, A.; Meshkov, G. Femtoscan online software and visualization of nano-objecs in high-resolution microscopy. *Nanoindustry Russia. Technosphera JSC* **2018**, *6*, 414−416.

https://doi.org/10.1021/acsomega.4c03152
ACS Omega 2024, 9, 43376−43384